Device

Article

Soft intelligent systems based on stretchable hybrid devices integrated with machine learning

Graphical abstract

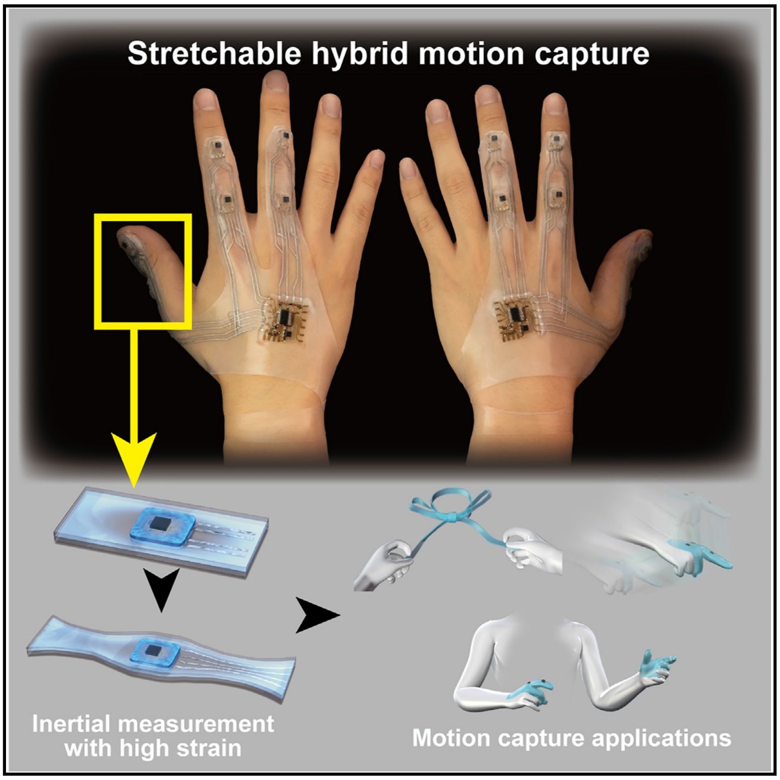

Highlights

- Highly stretchable hybrid devices fabricated and integrated into machine learning
- Intelligent systems with fabricated devices under large deformation demonstrated
- 10 knots, 26 finger-written alphabets, and 65 sign language words classified
- The findings will help to expand the applicability of stretchable electronics

Authors

Yuji Isano, Maika Takaya,
Yuta Kurotaki, ..., Tomoki Hamagami,
Kentaro Kuribayashi, Hiroki Ota

Correspondence

ota-hiroki-xm@ynu.ac.jp

In brief

Stretchable hybrid motion captures were developed by introducing rigid inertial sensors into a stretchable device using a structure with stepwise changes in stiffness, and stable measurement was realized at >150% elongation. Data collected by developed devices were processed using a machine learning algorithm to classify the 10 knot shapes, 26 finger-written alphabets, and 65 American Sign Language words. The findings will help to expand the applicability of integrated systems of flexible materials, highly precise and multifunctional hard electronics, and machine learning.

Isano et al., 2024, Device *2*, 100496
September 20, 2024
https://doi.org/10.1016/j.device.2024.100496

CellPress

Please cite this article in press as: Isano et al., Soft intelligent systems based on stretchable hybrid devices integrated with machine learning, Device (2024), https://doi.org/10.1016/j.device.2024.100496

Device

CellPress
OPEN ACCESS

Article

Soft intelligent systems based on stretchable hybrid devices integrated with machine learning

Yuji Isano,[1] Maika Takaya,[1] Yuta Kurotaki,[1,2] Ryosuke Matsuda,[1] Yusuke Miyake,[2] Tamami Takano,[3] Yutaka Isoda,[3] Tomoki Hamagami,[4] Kentaro Kuribayashi,[2] and Hiroki Ota[1,3,5,6,*]

[1]Department of Mechanical Engineering, Yokohama National University, 79-5, Tokiwadai, Hodogaya-Ku, Yokohama, Kanagawa 240-8501, Japan

[2]GMO Pepabo, Pepabo R&D Institute, 26-1, Sakuragaoka, Shibuya Ward, Tokyo 150-8512, Japan

[3]Graduate School of System Integration, Yokohama National University, 79-5, Tokiwadai, Hodogaya-Ku, Yokohama, Kanagawa 240-8501, Japan

[4]Graduate School of Engineering Science, Yokohama National University, 79-5, Tokiwadai, Hodogaya-Ku, Yokohama, Kanagawa 240-8501, Japan

[5]Institute for Multidisciplinary Sciences, Yokohama National University, 79-5, Tokiwadai, Hodogaya-ku, Yokohama, Kanagawa 240-8501 Japan

[6]Lead contact

*Correspondence: ota-hiroki-xm@ynu.ac.jp

https://doi.org/10.1016/j.device.2024.100496

THE BIGGER PICTURE Shape measurement of stretchable devices is more compatible with statistical processing by machine learning than kinematic analysis. Current stretchable sensors have low stability to repeated deformation, making collecting abundant training data difficult. Solid electronics-based sensors with high accuracy and stability reduce the device deformability due to stiffness mismatch with the elastic material. In this study, a rigid inertial sensor was introduced into a stretchable device using a multi-layered protective structure with stepwise changes in stiffness, and stable measurement was realized at >150% elongation. Machine learning processed the data collected with the device to recognize 10 knot shapes and classify 26 finger-written alphabets and 65 American Sign Language words. The findings open the possibility of realizing new systems by integrating flexible materials, highly precise and multifunctional hard electronics, and statistical processing by machine learning.

SUMMARY

Stretchable hybrid devices containing rigid sensing elements instead of stretchable sensors can acquire a wide variety of data with high repeatability, enabling the realization of intelligent systems with machine learning. However, integrated systems have limited applicability due to the low deformation tolerance of devices that contain elements of different stiffnesses. This paper presents the fabrication of highly stretchable hybrid devices and their integration into machine learning to demonstrate intelligent systems with stretchable hybrid devices under large deformation. Both three-layer protective structures and liquid metal paste wirings on the stretchable hybrid device with rigid inertial sensors enable it to transmit data stably at 150% elongation. The device is integrated with a machine learning system to classify 10 types of knots, finger-written alphabets, and 65 words of sign language, achieving classification accuracies of 86%, 98%, and 95%, respectively. These findings will help expand the applicability of stretchable electronics.

INTRODUCTION

Stretchable devices are being developed extensively by focusing on the characteristics of following a highly flexible and deformable living body.[1] Such devices are commonly used in wearable health monitoring,[2–5] motion measurement,[6–11] and soft robotics[12,13] to acquire physical and bioelectrical information.

Processing and interpreting data obtained from stretchable sensors are indispensable to realize practical systems using stretchable devices. A fully deformable device has high degrees of freedom, making it difficult to mathematically model its shape based on its sensor outputs. Moreover, discerning the underlying meaning in the patterns of motion and bioelectrical potentials that can be interpreted by stretchable devices is crucial, and this cannot be accomplished via simple numerical processing.

Please cite this article in press as: Isano et al., Soft intelligent systems based on stretchable hybrid devices integrated with machine learning, Device (2024), https://doi.org/10.1016/j.device.2024.100496

Processing the data obtained from such stretchable devices is highly compatible with machine learning,[14,15] which can process a large number of parameters in a nonlinear and stochastic manner. The integration of stretchable devices and machine learning algorithms can enable intelligent systems that afford possibilities beyond numerical calculations, such as shape interpretations of elastic bodies,[16] hand motion estimation,[7,11] and speech inference using vibration and myoelectricity.[16,17]

Stretchable devices for integration with machine learning are generally equipped with flexible strain or pressure sensors or electrodes for acquiring biological potentials. However, the stability of the stretchable sensors used in these devices deteriorates over time due to inferior repeatability and undesired fluctuations in measurements caused by deformations.[18] This remains a major issue because machine learning systems require devices that can stably acquire a large amount of data.

Hence, stretchable hybrid devices that can combine stable data processing with sufficient deformability are attracting attention.[19] Stretchable hybrid devices comprise rigid integrated circuits (ICs) mounted on a highly deformable substrate connected to one another via stretchable interconnections. The rigid ICs enable digital conversion of the measured data on the device and low-noise communication.[20] Furthermore, the sensor IC based on solid-state electronics enables simultaneous measurements of multiple parameters with high repeatability and physical quantities that cannot be measured using soft sensors.

A stretchable hybrid device with a rigid IC as the sensing element instead of a stretchable sensor has high stability and can collect a variety of data, making them suitable for integration with machine learning systems. However, systems that use stretchable hybrid devices have limited applicability when compared with those using stretchable sensors, and measurements can be performed only for small deformations, such as pulse rate[21,22] and bioelectrical potential.[3,4,23–26]

This limitation can be attributed to the lack of deformation capability, preventing their use in objects that undergo large deformations. The difference in the elastic modulus between the rigid element and deformable material in stretchable hybrid devices causes junction rupture[24,27–29] and subsequent disconnection of the stretchable wiring, resulting in limited overall stretchability of the device. This has prevented the application of machine learning systems using stretchable hybrid devices to a wide range of objects. To expand the potential of such systems, the development of new stretchable hybrid devices with high deformability is necessary, which can be applied to objects with large deformations and demonstrate their integration with machine learning systems.

In this study, we developed a system that integrates stretchable hybrid motion capture using rigid 6-axis inertial measurement units (IMUs) and machine learning for data analysis. Stretchable hybrid devices that can maintain stable communication performance for 150% elongation were constructed by using heterogeneous-rigidity protection to prevent breakage between the hard-soft interface and highly deformable wiring using liquid metal (LM) paste[30]; the heterophasic LM contains monophasic LM and solid particles. The shape and trajectory estimation of the device was achieved by analyzing acceleration and angular velocity data acquired by the stretchable hybrid device using machine learning. Three tasks were accomplished to demonstrate the system that integrates the stretchable hybrid device and machine learning for highly deformable objects: self-shape estimation of knots with large device deformation, recognition of writing in the air (including parallel movement components that are difficult to read with flexible sensors), and sign-language recognition that classifies several similar motions. Experimental results indicate that highly deformable objects can be effectively analyzed by integrating a stretchable hybrid device comprising a rigid IC and heterogeneous-rigidity structure with machine learning.

RESULTS

Shape and motion recognition system with highly stretchable hybrid device

The developed device is shown in Figure 1A. Multiple IMUs were mounted on a substrate made of Ecoflex, a stretchable silicone rubber. Heterogeneous-rigidity protective structures composed of three materials with different elasticities were used to incorporate the non-stretchable circuits into the stretchable substrate (Figure 1B). The heterogeneous-rigidity protective structure contains three layers: a hard layer for protecting the electrical contacts between the hard material and elastic wiring, an intermediate layer for mitigating drastic strain changes around the circuit board, and a soft layer for ensuring high elasticity. This structure prevented rupture between the rigid element and soft layer, even at 150% elongation.

LM paste was used for the electrical connection between the hard elements. Despite the high stretchability and conductivity of monophasic Galinstan, it cannot be wired easily on a stretchable substrate owing to its high surface tension; moreover, it breaks easily at the hard-soft interface.[20] The viscosity of the Galinstan paste was improved by mixing it with metal powder, allowing its direct application to flexible substrates. The paste has a lower surface tension, preventing cohesion and wire breakage at the material interface. The combined effect of suppressing the strain concentration by the heterogeneous-rigidity protection and durability of the LM paste wiring enables the realization of stretchable hybrid devices that can operate even at 150% elongation.

The developed device was used to collect motion data, and machine learning was used to estimate the shape and motion of the device. Three tasks are demonstrated: self-shape estimation of knots, recognition of writing in the air, and sign-language recognition (Figure 1C).

Incorporation of non-stretchable circuits into stretchable substrates

The strain distribution of a one-element device with a heterogeneous-rigidity protective structure (Figure 2A) under tensile strain is compared with that of the device with only a circuit board and soft layers (Figure S1).

The structure with the elastic modulus decreasing in steps, centered on the rigid circuit board, prevents strain concentration around the board. This suppresses the strain gradient around the hard substrate even at 100% elongation, preventing rupture caused by the difference in elastic modulus. By contrast, a

Please cite this article in press as: Isano et al., Soft intelligent systems based on stretchable hybrid devices integrated with machine learning, Device (2024), https://doi.org/10.1016/j.device.2024.100496

CellPress
OPEN ACCESS

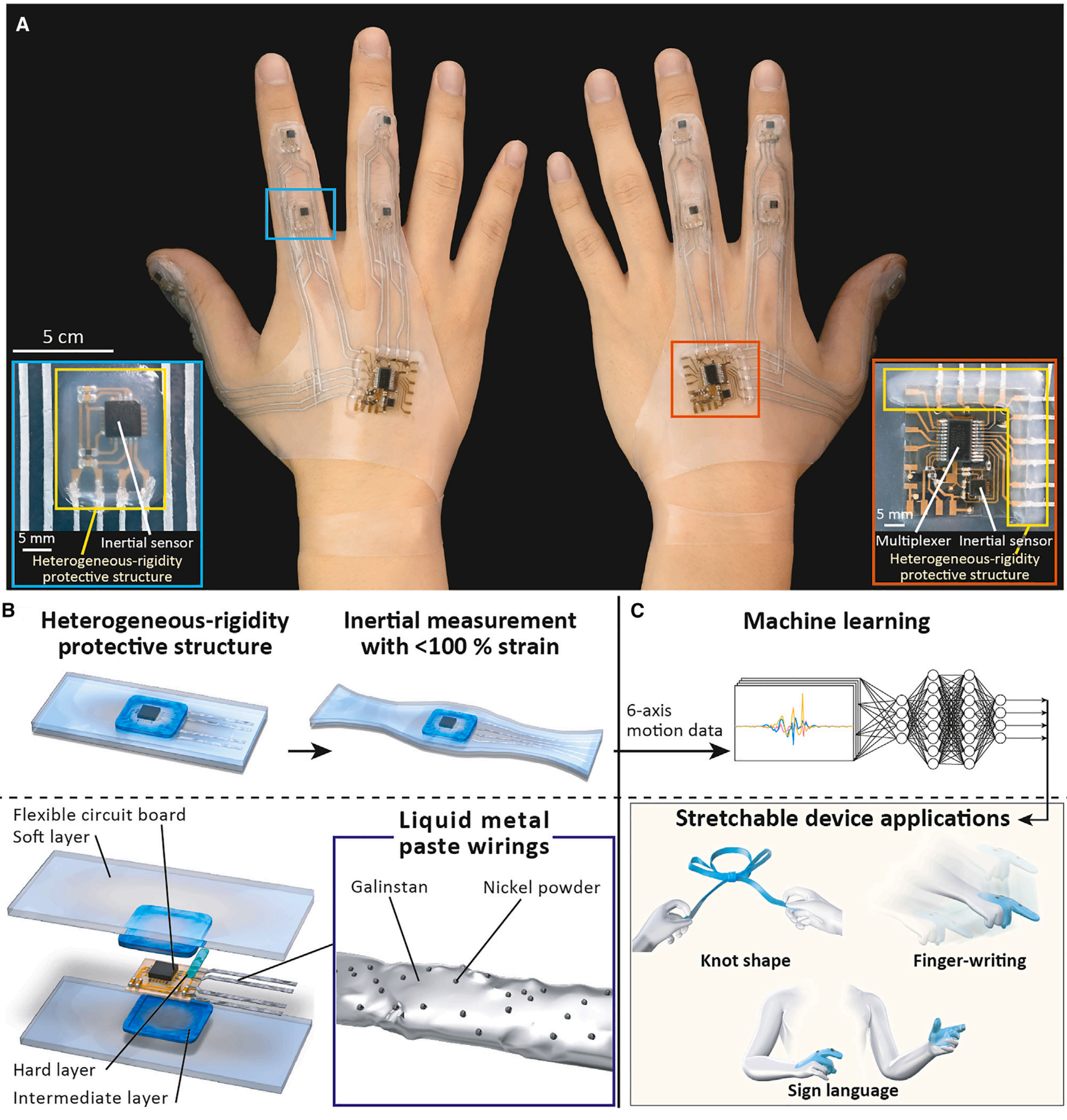

Figure 1. Integrated system using highly stretchable hybrid device and machine learning

(A) Photographs of the developed stretchable hybrid device. Blue rectangle: magnified view of the area around the IMU. Orange rectangle: magnified view of the area around the multiplexer. Rigid ICs mounted on flexible circuit boards placed on highly deformable substrate. Circuit boards protected by heterogeneous-rigidity structures to improve tolerance to elongation. LM paste used to incorporate stretchable wiring to prevent disconnection on hard-soft heterojunctions.

(B) Schematic of heterogeneous-rigidity protection. Circuit board protected by 3 layers: hard layer to protect connections with stretchable wirings, intermediate layer to mitigate strain concentration, and soft layer as a stretchable sealing layer. Highly conductive LM paste made by combining LM and micro-powder of nickel used for stretchable wiring.

(C) Highly deformable applications realized by integration with machine learning. Artificial neural networks trained using 6-axis inertial datasets measured by stretchable hybrid devices to demonstrate 3 types of classification—knot-shape identification, finger-writing recognition, and sign-language recognition.

Please cite this article in press as: Isano et al., Soft intelligent systems based on stretchable hybrid devices integrated with machine learning, Device (2024), https://doi.org/10.1016/j.device.2024.100496

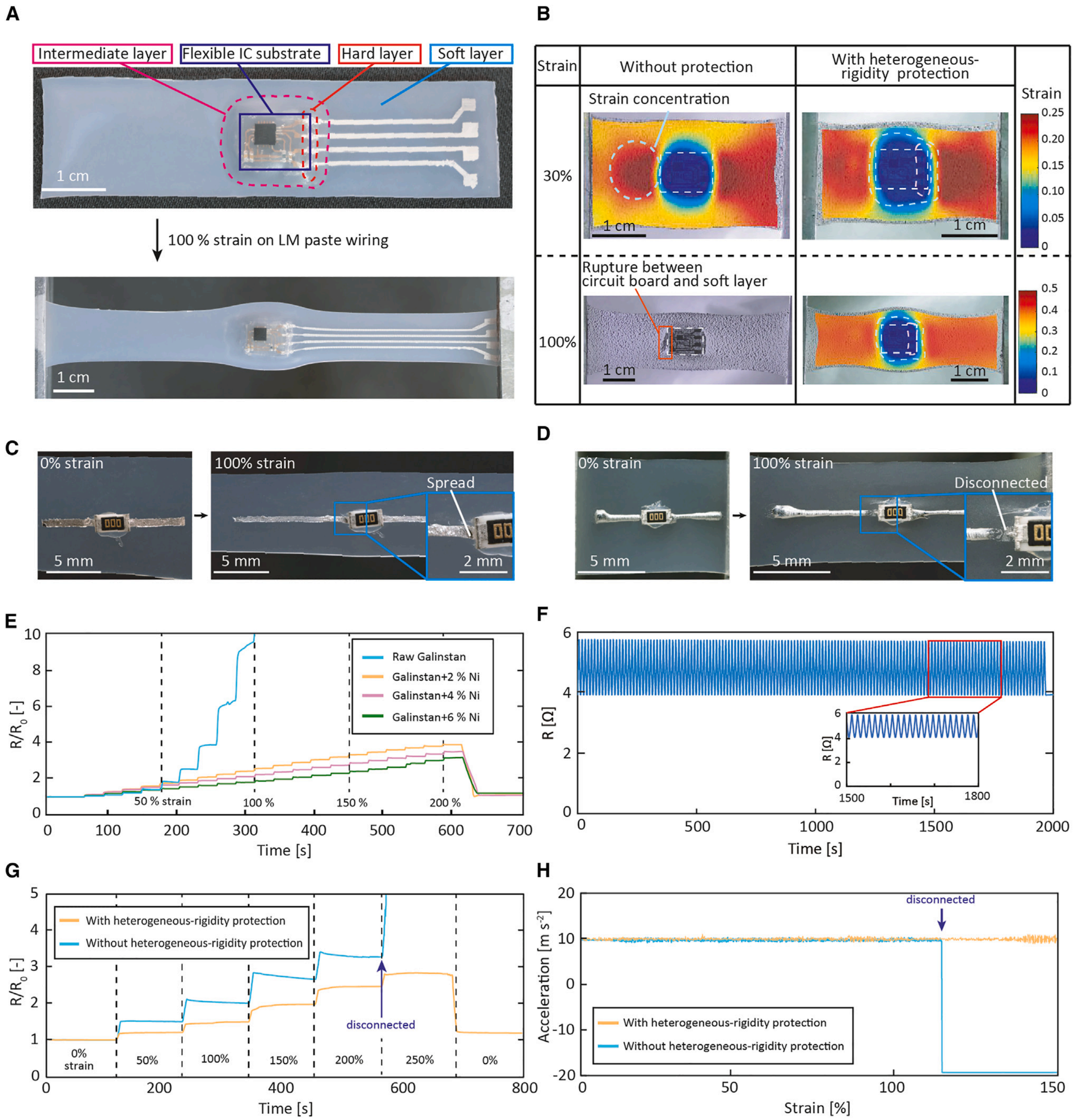

Figure 2. Characteristics of developed stretchable hybrid devices

(A) Single-element stretchable hybrid device for characterization. IMU and some passive elements mounted on a flexible substrate placed on a heterogeneous-rigidity protective substrate. Device stretched from a relaxed state to 100% strain on LM wirings.

(B) Strain distribution analysis of single-element device using digital image correlation (DIC). Device without protection (left) showed strain concentration near the circuit board at 30% strain, resulting in rupture at 100% strain. The device with protection (right) did not rupture at 100% strain.

(C and D) Wirings using (C) LM paste and (D) monophasic Galinstan connected to chip resistor. LM paste wirings did not disconnect at 100% strain. Blue rectangle: magnified view.

(E) Electrical resistance of the LM paste and monophasic Galinstan wirings connected to the chip resistor. LM paste wirings show a more stable increase in resistance with strain than monophasic Galinstan.

(legend continued on next page)

device with only a circuit board and soft layer exhibits strain concentration around the substrate at 30% strain and rupture of the substrate-soft layer adhesion at 100% strain (Figure 2B). These comparisons indicate that the heterogeneous-rigidity protection can mitigate the large strain gradients around the non-stretchable substrate and prevent deformation-induced rupture.

The elongation limit of the LM paste (Figure 2C) wiring is compared with that of monophasic LM (Figure 2D). The LM paste was applied to a chip resistor (Figure 2C), and the wiring was strained by 100%. The wiring remained connected with the chip resistor, as its high viscosity caused it to spread. By contrast, the contact between monophasic LM and the chip resistor was easily broken due to the high surface tension of monophasic LM (Figure 2D). The LM paste showed stable resistance change up to 200% strain (Figures 2E and S2A), whereas the monophasic LM showed a resistance change of nearly 10 times at approximately 100% strain.

The formation of a paste with high viscosity by mixing Ni powder with LM has been reported.[30] The increase in viscosity reduces the effect of the surface tension of the LM and improves wettability to the substrate. This is considered to suppress the self-agglomeration of the LM during elongation of the wiring, thereby improving the breaking limit strain of the wiring. The LM paste with less nickel powder showed a larger resistance change because its properties are closer to those of monophasic LMs. Based on these results, an LM paste mixed with 6% nickel powder by mass was used for a practical device for the convenience of device fabrication. The wiring of the LM paste alone, which was not connected to the chip resistor, showed almost no change in resistance after 100 cycles of 100% strain (Figure S3).

The combination of LM paste wiring and heterogeneous-rigidity protection can ensure a stable connection with rigid elements even under large deformations. The resistance between the LM paste wiring and circuit pattern on the rigid substrate was measured. The resistance was stable within a narrow range even after the application of 150 cycles of 100% strain (Figures 2F and S2B). Additionally, the wiring resistance with the heterogeneous-rigidity protection changed only approximately three times even at 250% elongation (Figures 2G and S2C), whereas the wiring without the protection broke under 250% strain. z axis acceleration measurements were performed while gradually applying strain to the stationary device. The device with the protective structure continued to communicate even at 150% strain, but that without the protective layer lost communication at approximately 110% strain. Both devices had a constant value of gravitational acceleration, which did not change with the strain (Figures 2H and S2D). In addition, tensile strain had no effect on the measurements during the tests conducted under constant angular velocity and acceleration using a rate table (Figure S4; Note S1; Tables S1 and S2). Thus, the combination of a heterogeneous-rigidity protective structure, LM paste wiring, and sensor IC capable of digital communication can ensure stable measurements regardless of the deformation state.

LM paste wiring remains conductive even when the interface between the hard and soft surfaces breaks owing to the spreading of the paste. Stable communication in this state is difficult due to shorts in the adjacent wiring caused by the spreading paste and differences in resistance between the wirings. This is considered the reason for the much lower disconnection strain of the IMU than that of a single wiring.

Designs to protect the elements with two types of rigid structures have been reported,[19,24,29,31] but these become ineffective when stretching exceeds 80%. Although protective layers that can withstand uniaxial tension of 200% or more by optimizing the two-layer protective structure have been reported,[22] the complex structure and large protective layer make its implementation difficult in places with limited area, such as fingertips. The application of the method of mounting only the IC on the stretchable material[20,21] was limited to 80% elongation because the wiring was made of monophasic LM. In our study, communication with the IC was maintained even at 150% elongation because of the heterogeneous-rigidity protection, which prevented physical damage, and LM paste, which stabilized the electrical connection. These characteristics enabled the device to withstand large deformations and allowed it to be mounted on a small area such as the fingertip or a thin ribbon.

Estimation of knot shape with ribbon-like device

The incorporation of IMUs into stretchable devices using a rigid-soft composite structure enables the acquisition of multidimensional trajectory information, which cannot be achieved using existing soft strain and bending sensors alone. The obtained trajectory information can be processed by machine learning to estimate the shape that will be formed in a specific procedure. In the present study, a knot-shape-prediction system based on the motion history of both ends of a ribbon was developed as a proof of concept for a shape-prediction system using a stretchable hybrid device.

The ribbon device for trajectory acquisition (Figure 3A) was fabricated by mounting an IMU protected by heterogeneous-rigidity protection on both ends of a silicone band and connecting them with LM paste wiring. To swap the order of the LM interconnections, the soft layer material was used as insulation for the crossing interconnections. The stretchable substrate and heterogeneous-rigidity protection of the device enable it to withstand tension and compression when a ribbon is tied together, and to acquire stable inertial data even under large deformations.

Time series data of the acceleration and angular velocity along each of the three axes were acquired from the two sensors when the ribbon devices were tied (Figure S5). These knot data were classified using a one-dimensional convolutional neural network (1D CNN) (Figure 3B). CNN optimization was performed

(F) Resistance change between LM paste wiring and circuit board with protective structure when wiring was stretched 100% repeatedly; no significant increase in resistance is observed after 150 cycles.

(G) Comparison of resistance change between LM paste wiring and circuit board under strain with and without protective structure.

(H) z axis acceleration measurements of the single-element device under strain. Device with a protective structure accurately outputs acceleration of gravity even when the wiring is subjected to 150% strain.

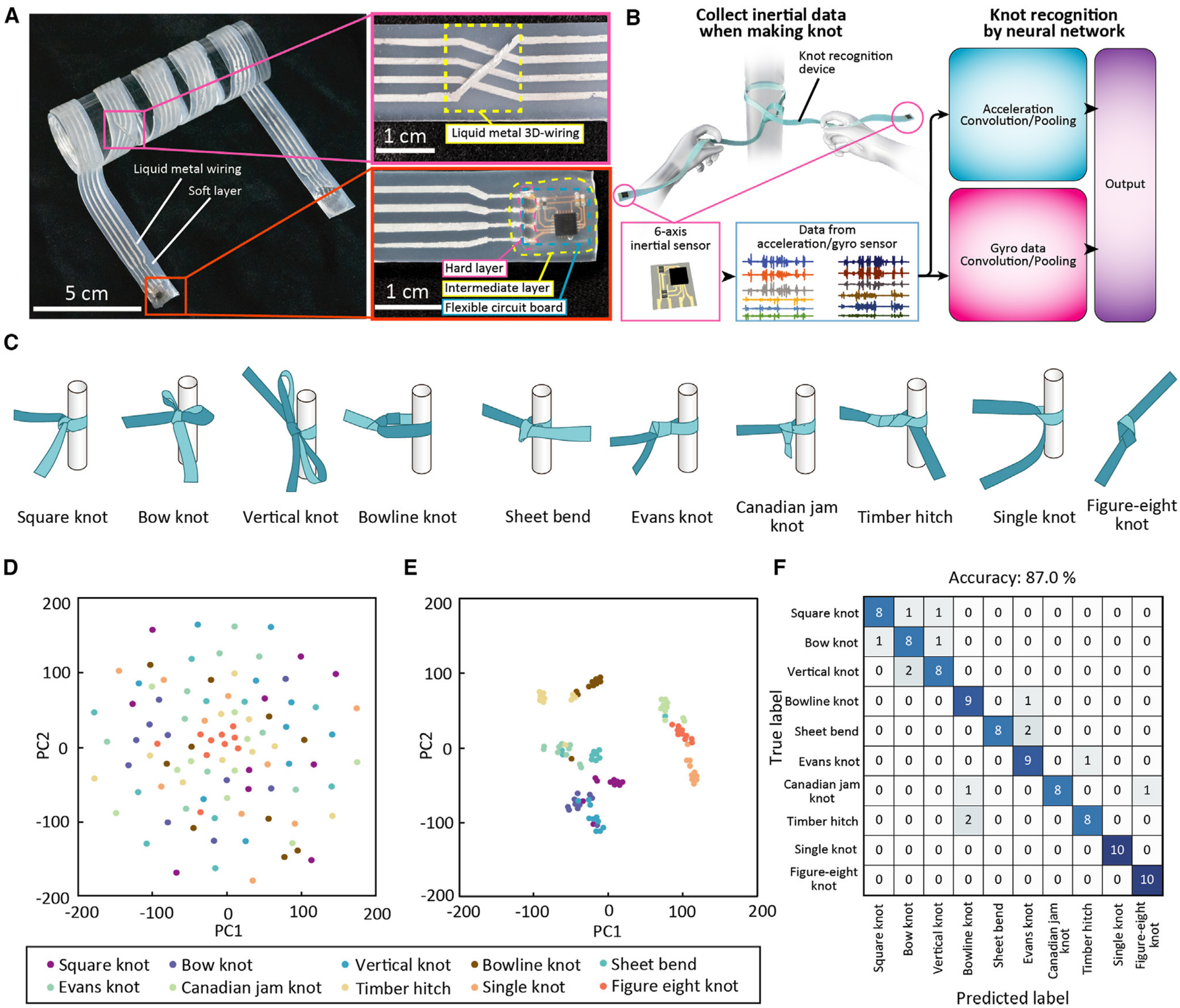

Figure 3. Knot-shape classification system using stretchable hybrid device and machine learning

(A) Photograph of the knot-shape recognition device. IMUs protected by heterogeneous-rigidity protection were installed at both ends of a stretchable ribbon-like device. The elements were connected by LM paste wirings. LM paste was applied to the 3D wiring to obtain 3D intersections of the wiring.

(B) Overview of the knot classification system flow. Inertial data extracted from 6-axis sensors when the devices were tied together were processed using a CNN to classify the 10 different knots.

(C) Illustrations of 10 knot shapes.

(D and E) Clustering results using (D) data from the input layer and (E) data immediately before the output layer. (D) The input layer data show a scattered distribution, whereas (E) the data just before the output layer are clustered by class.

(F) Confusion matrix for classification of 10 types of knots. The classification accuracy is 87%.

(Figures S6–S8; Table S3; Note S2) to classify the 10 types of knots, as shown in Figure 3C. Subsequently, the model was trained to create a classification system (Figure S9).

Data were visualized by clustering to verify the classification ability of the trained neural network. An almost disorderly scattering of the data was observed in the clustering of the input layer data (Figure 3D). By contrast, 10 clusters of the data were formed immediately before the output layer; however, some of the data were mixed (Figure 3E). The important features were extracted from the inertial data of the tying motion using the CNN.

The validation results using the test data are shown in Figure 3F. The prediction accuracy is 0.87. High prediction accuracy was achieved for all knots except for the bow and vertical knots, which differed only in the direction of motion and were therefore misidentified. Additionally, real-time classification was performed by immediately acquiring the tying acceleration data, as shown in Video S1. Although shape recognition using IMU has been reported,[32] implementation on a stretchable board has not yet been achieved. Hence, deformable strain sensors[33–35] were considered a more promising option for shape estimation.

Please cite this article in press as: Isano et al., Soft intelligent systems based on stretchable hybrid devices integrated with machine learning, Device (2024), https://doi.org/10.1016/j.device.2024.100496

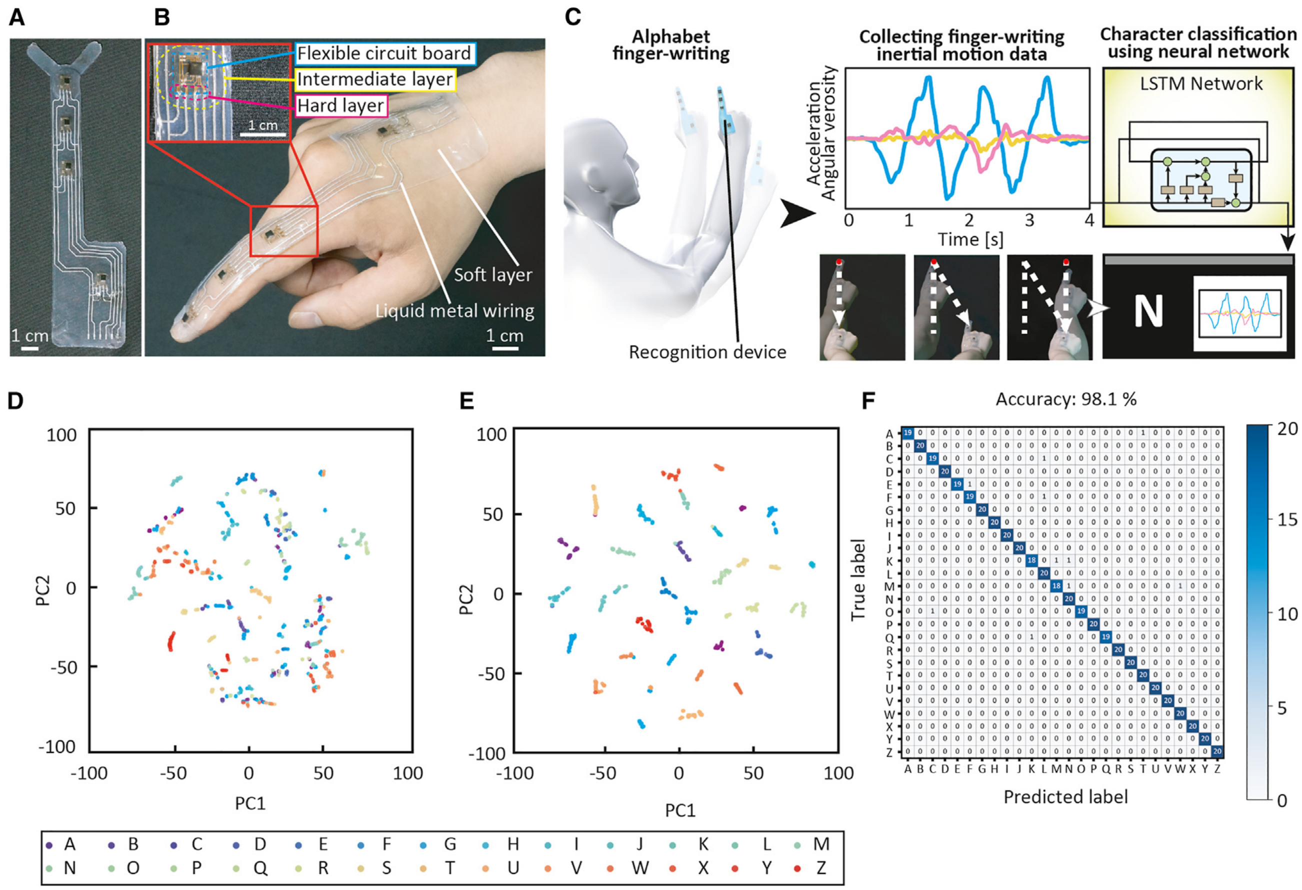

Figure 4. Finger-writing classification system using stretchable hybrid device and machine learning

(A) Photograph of the finger-writing recognition device. IMUs protected by heterogeneous-rigidity structures are placed on a stretchable substrate shaped to fit easily on the hand. The elements are connected by LM paste wirings.

(B) Photograph of the device attached to the hand. Four IMUs were mounted between the joints of the index finger and back of the hand.

(C) Overview of the finger-writing classification system flow. Six-axis inertial data from the IMU during writing of the alphabets in the air were used to train the LSTM network to classify 26 letters of the alphabet.

(D and E) Results of clustering using (D) data from the input layer and (E) data immediately before the output layer. The input layer shows a scattered distribution (D), whereas the data immediately before the output layer shows clustering by class (E).

(F) Confusion matrix in the classification of 26 alphabets. The classification accuracy is 98.1%.

In this study, an IMU mounted on a stretchable device was used in a self-shape-prediction system to prove the possibility of estimating the overall shape from the local acceleration of the device. The result can be applied to systems such as soft robots, where measuring all the moving parts is impossible, to estimate the shape through local measurements. Although direct shape measurement is not possible, this problem can be solved by applying a system that recognizes the deformation of magnetic polymers using microelectromechanical systems magnetic sensors and machine learning.[36]

Finger-writing alphabet recognition by finger movement analysis

Stretchable devices are generally used in wearable applications on the human body. Hand motion capture has been in high demand in recent years. Stretchable hand motion capture can recognize finger shape and motion using stretchable bending sensors[11,37,38] and electromyography,[7] but these methods have difficulty in reading parallel movements without finger bending. In our study, IMUs were attached to the finger using a stretchable and adherent device to read alphabets written in the air, which cannot be read with a bending sensor alone.

A heterogeneous-rigidity device for finger-writing character recognition is shown in Figure 4A. The inertial data of the finger movements were read by four IMUs mounted on the index finger and the back of the hand (Figure 4B). As shown in Figure 4C, the inertial data were recorded by writing letters of the alphabet in the air with the device attached (Figure S10). The range of the finger-writing motion was automatically detected using the acceleration threshold (Figure S11). The data were processed using zero padding to unify the lengths of the data. Machine learning was conducted using the recorded data to realize real-time finger-writing recognition of alphabetical letters (Figure 4C).

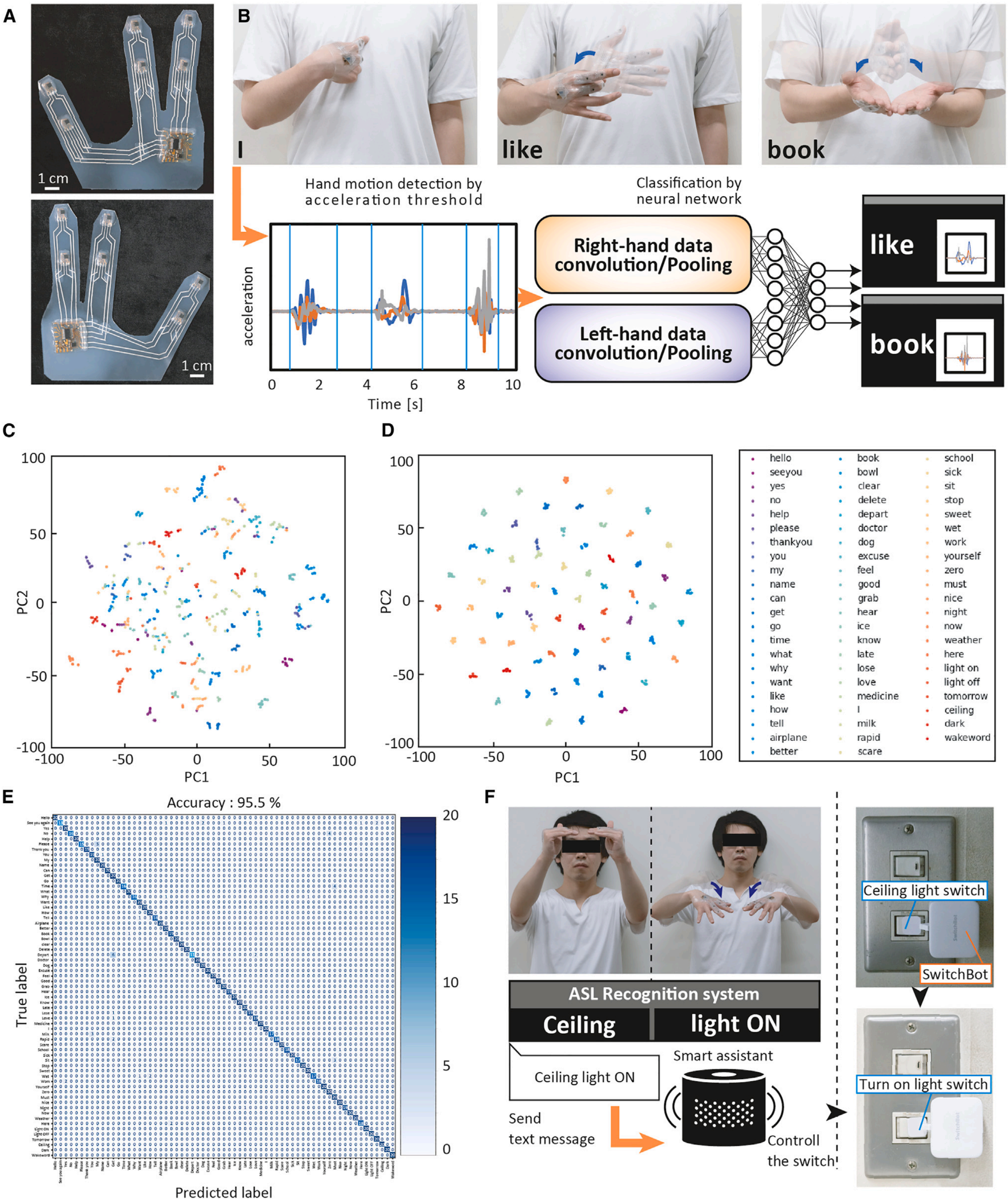

Figure 5. Sign-language recognition system using an integrated stretchable hybrid device with machine learning

(A) Photograph of the sign-language recognition device. Seven IMUs are mounted on the thumb, index finger, middle finger, and back of the right and left hands.

(B) Overview of the sign-language recognition system flow. The motions made in sign language are determined using the acceleration threshold.

(legend continued on next page)

A neural network with a long-short-term memory (LSTM) model was employed to classify the inertial data of the finger-written letters. The LSTM model is suitable for learning time-series data and is therefore effective in recognizing alphabetic characters with a fixed stroke order. The model was optimized in terms of the number of layers, number of units, and number of features to be used (Figures S12 and S13; Note S3, Table S4). The optimized model was then trained to create a classification system (Figures S14 and S15; Table S5). During the training process of the model, sharp fluctuations were observed in Loss and Accuracy, typical of those observed at approximately 280 epochs. In the end, the classification accuracy for the training and validation data converged to approximately 98%.

Clustering was performed for the input layer (Figure 4D) and the data after passing through the second LSTM layer (Figure 4E). Unlike those in knot classification, small clusters of the letter units were formed from the input data in the case of finger-writing. This suggests that the inertial data of finger-written alphabetical characters with a uniform stroke order have similar features for each character. Upon passing through the neural network, the data exhibited more than 26 clusters. Although some characters were divided among multiple clusters and different characters were mixed within a cluster, the neural network improved classification performance.

The classification accuracy was evaluated using the test data, and a high accuracy of 98.1% was observed (Figure 4F). Furthermore, as shown in Video S2, real-time sequential recognition of multiple characters was also achieved. The automatic detection system of the writing conditions using the acceleration thresholds enables recognition of the boundaries between the characters, thus achieving character segmentation with a small amount of computation.

A model for processing multidimensional time-series data based on the Vision Transformer (ViT) was also constructed, and its performance is compared with that of LSTM (Figures S16–S19; Note S4). Based on the results, the classification accuracy of the ViT-based model is 91.7%, slightly lower than that of the LSTM, but the model achieved comparable performance with one-fourth of the number of training epochs of LSTM.

Finger character recognition using machine learning and multiple placements of IMUs on the finger using heterogeneous-rigidity protection and stretchable wiring was demonstrated. Although finger-writing recognition using only a bending sensor has been reported,[39] the findings of this study are better than those of the previous study in terms of the number of recognizable characters and recognition accuracy. These results validate the usefulness of the IMU and its ability to read parallel movements. Compared with existing finger-writing recognition systems with a single IMU,[40,41] the proposed method requires numerous sensors and extensive wiring, resulting in a larger device. Nevertheless, the proposed method can recognize finger-written characters regardless of the shape of the finger due to multiple sensors mounted on each joint. In addition, the device can be wired from the fingertip to the back of the hand. Therefore, high functional expandability is expected, allowing large computational elements and batteries that do not fit on the finger to be mounted on the back of the hand.

Further investigation is needed on the generalization performance of the machine learning model. The sharp fluctuations in loss that occur during training suggest that the LSTM model may be overfitting certain training data. In contrast, such events are not observed in the ViT-based model trained using the same training data (Figure S19). This suggests that the phenomenon is caused by overfitting LSTM models with some training data, which perform complex error back-propagation calculations, including recursion. To improve generalization performance, future research needs to develop larger datasets for training and validation and study models in more detail.

Recognition of American Sign Language (ASL)

Sign-language recognition systems using wearable devices and machine learning have been developed using various methods.[7,11,42,43] A deformable device that does not interfere with hand movements is desirable, considering user comfort. However, soft strain sensors[11,38] provide information on only the shape of the hand, limiting the types of signs that can be read. Integrating the heterogeneous-rigidity device developed in this work into a sign-language recognition system enables the system to be highly comfortable to wear and to acquire many desirable features.

Sign-language recognition devices were equipped with seven IMUs on the thumb, index finger, middle finger, and back of the hand, protected by a heterogeneous-rigidity structure (Figures 1A and 5A). An I2C multiplexer was mounted on the back of the hand to centralize communication with multiple sensors. The motion data of the signs acquired with this device were used for machine learning to achieve word recognition in American Sign Language (ASL) (Figure 5B). The target vocabulary was 65 words (Figure S20), containing 50 words considered to be frequently used in a previous study[42] and 15 words used as input for Internet of Things devices.

The 1D CNN was selected as the neural network model for sign-language recognition, and the model was optimized (Figures S21 and S22; Note S5) to determine the shape of the model (Figure S23; Table S6). In addition, training data were augmented (Figure S24; Note S6) to deform the data in the temporal direction to accommodate different speeds of sign-language gestures.

Clustering was used to visualize the recognition performance of the trained (Figure S25) model. Clustering was performed on the input (Figure 5C) and output data of the full concatenation layer just before the output layer (Figure 5D). The results showed that the word-by-word patterns that were only slightly visible in

(C and D) Results of clustering using (C) data from the input layer (scattered distribution) and (D) data immediately before the output layer (clustered by class).
(E) Confusion matrix for the classification of 65 words in ASL. The classification accuracy is 95.5%.
(F) Communication with a smart assistant using the sign-language recognition system. Signs are converted into text by the recognition system and sent to the smart assistant. The ceiling lights were controlled via the smart assistant.

the input data were completely separated in the output data of the full concatenation layer. Validation with the test data showed a 95.5% correct response rate (Figure 5E). As presented in Note S5, the recognition performance for signs made at different speeds was slightly improved through data expansion (Tables S7 and S8). Additionally, a word separation system that uses acceleration thresholding (Figure S11) was utilized to segment continuous sentences into words and convert them into text in real time (Video S3).

As a practical example of the ASL recognition system, smart assistant software was controlled through sign-language input (Figure 5F). Indications to the smart assistant can be distinguished by treating the finger-snapping action as a wake-up instruction for the smart assistant. The recognized sentences were sent to the smart assistant on the local area network, which responded and controlled the lights using an existing commercial system (Figure S26; Video S4). Although smart assistants have been developed by various companies, their input methods are limited to voice or text. The integration of gesture interfaces and smart assistants with wearable devices provides a new communication system for both signers and speakers.

Even though the concept of a communication system with a smart assistant using a sign-language recognition glove has been presented, many challenges exist in its actual use. A word segmentation system that uses acceleration thresholds can result in false positives, where unrelated actions are recognized as signs when the user is supposed to sign during everyday activities. The problem can be solved by developing a statistical word segmentation system that uses inertial data from sign language and everyday movements instead of a deterministic process that uses acceleration thresholds. Additionally, sign language in motion results in different data than sign language at rest, primarily because the inertial data from hands are affected by the motion of the entire body. This problem could be solved if a dataset of signs in daily activities could be used to train the model. Thus, a large dataset of hand movements and sign language in daily life is required to improve the system to a level where it can be used in real life. The development of a stand-alone system with wireless communication based on the device proposed in this study could realize the production of such a large dataset. In addition, a latency exists of approximately 3 s from the end of sign language to the display of the word, as shown in Videos S3 and S4. This entails a 1-s waiting time for word-end detection, as shown in Figure S11, 0.18 s of preprocessing and estimation time, and 1.83 s of screen display processing. To eliminate this delay, it would be effective to use a more efficient training model, reduce the drawing time, and fundamentally improve the word segmentation system.

Most sign-language recognition systems using stretchable devices are limited to static shape detection,[11,43,44] whereas those that achieve dynamic sign-language recognition are rigid[45,46] and interfere with hand motions. The system reported in this study solves these problems and achieves both high hand adhesion of the device and highly accurate dynamic sign-language recognition. Additionally, the system achieved the same recognition performance with fewer sensors by using multidimensional sensing with IMU when compared with the sign-language recognition system that integrates triboelectric nanogenerator sensors with a CNN.[42] By contrast, gestured sentences were not segmented through machine learning in this study. This is a critical aspect in applying the systems to practical uses, and an improved system should be developed in the future.

DISCUSSION

In this study, stretchable hybrid devices with large deformation capability were developed and integrated with machine learning to realize three types of classification systems. With a three-layer heterogeneous-rigidity structure and highly stretchable LM paste wiring, the device with an IMU achieved uninterrupted communication even at 150% strain. Devices with heterogeneous-rigidity structures were applied to ribbon devices, finger-writing recognition devices, and sign-language recognition devices, where they continuously recorded motion data even under high deformation. The acquired motion data were classified via machine learning, and the classification accuracies were 87%, 98%, and 96% for knot shape, finger-writing, and sign language, respectively. These results indicate that the integration of a stretchable hybrid device comprising a rigid IC and heterogeneous-rigidity structure with machine learning can effectively analyze largely deformable objects. These demonstrations indicate that the integration of stretchable devices and machine learning systems can be effectively realized based on devices that simultaneously realize measurement and large deformation using highly stretchable materials and rigid ICs.

The results of this study, which integrated intrinsically stretchable wiring and rigid devices, can serve as a reference for implementing a machine learning system for a largely deformable object. The advantages of integrating stretchable devices and rigid elements include signal stabilization by digital conversion near the sensor and simultaneous mounting of different types of devices by unifying the communication protocols. As an extension of this research, an ultrasonic rangefinder can be mounted on a sign-language device to collect the relative coordinate data between the hand and body for sign-language recognition. By contrast, heterogeneous-rigidity-structure devices pose challenges such as reduced deformability of the entire device with an increase in the number of mounted elements and difficulty in establishing a mass production process line. These problems can be solved by developing a technology to efficiently form a minimal heterogeneous-rigidity protective layer using multi-material 3D and other technologies. It is expected that new devices that integrate circuit elements, such as ultrasonic transducers, photodiodes, analog-to-digital converters, and operational amplifiers, which have not yet been made stretchable for practical use, will be developed for applications where large deformations are expected.

EXPERIMENTAL PROCEDURES

Resource availability

Lead contact

Requests for resources should be directed to the corresponding author and lead contact, Hiroki Ota (ota-hiroki-xm@ynu.ac.jp).

Materials availability

This study did not generate new unique reagents.

Data and code availability

All original code is available in this paper's supplemental information.

Any additional information required to reanalyze the data reported in this paper is available from the lead contact upon request.

Fabrication of flexible circuit boards

The circuit pattern on the flexible substrate was fabricated using a photolithographic etching process on a copper-clad film (L71KT, total thickness 45 μm/copper layer thickness 25 μm, Arisawa Manufacturing). Upon spin coating a photoresist (AZ 1500, Merck) on the copper-clad film, the resist was patterned using an exposure system (M-2L, MIKASA) and a photomask. The patterned resist was developed using a developer (NMD-3, Tokyo Ohka Kogyo), and the unwanted copper was corroded via an etching process to fabricate the circuit board pattern. Gold (100 nm) was then deposited on the area of contact with the LM paste wiring to improve the wettability for the paste.

Chromium (10 nm) and gold layers (100 nm) were deposited on the back of the multiplexer substrate to form a double-sided circuit board. For the connection between the front and back, conductive silver paste (Dotite, Fujikura Kasei) was poured through holes formed on the substrate using a laser marker to form a conductive path. Subsequently, a 6-axis IMU (MPU6500, TDK Corporation), an I2C communication multiplexer (PCA9548A, Texas Instruments), and other passive elements were mounted on the substrate to fabricate a flexible circuit board (Figure S27A; Data S1 and S2).

Preparation of LM paste

LM paste was prepared by mixing Galinstan with nickel powder (3–7 μm, Alfa Aesar). The nickel powder was combined with Galinstan (15 g) at a constant mass ratio and mixed at 2000 rpm for 20 min using a planetary mixer (ARE-310, Thinky). The material was then sonicated with an ultrasonic probe (SFX550, Branson) to 6 kJ and left overnight to stabilize the physical properties, forming a paste.

Fabrication of heterogeneous-rigidity-structure devices

Stretchable devices with a heterogeneous-rigidity structure were fabricated according to the procedure shown in Figure S27. The soft layer was fabricated by molding silicone rubber (Ecoflex 00-50 [A:B = 1:1 weight ratio], Smooth-on) using a 3D-printed mold (Figure S27B(i); Data S3). The molding created a shallow indentation at the position of the sensor substrate (Figure S27B(ii)). A 50-μm-thick polyimide film was applied on the soft layer and cut using a laser marker (MD-T1000, Keyence) to form a stencil mask (Figure S27B(iii)). LM paste was applied over the stencil mask, and the mask was removed to fabricate the patterned stretchable wiring (Figure S27B(iv)). At the intersection of the wirings, an insulating layer was formed by dipping Ecoflex 00-50, and the LM paste was applied again using a stencil mask to fabricate the 3D intersecting wirings. After the wiring was completed, the flexible substrate with the mounted circuit elements was fixed to the soft layer using a silicone sealant (Dowsil 734, Dow Corning), which served as an intermediate layer (Figure S27B(v)). The circuit on the flexible substrate was then electrically connected to the LM paste wiring by applying LM paste from the top of the flexible board to the wiring (Figure S27B(vi)). Epoxy resin (JER 828:JER cure 3080 = 2:1, Mitsubishi Chemical), which is a hard layer material, was dropped onto the contact area between the LM paste wiring and flexible board and cured at 70°C for 3 h to form a hard layer (Figure S27B(vii)). Dowsil 734 was dripped around the flexible substrate for sealing (Figure S27B(viii)). Finally, the entire device, including the LM paste wiring, was encapsulated by spraying Ecoflex 00-50 (A:B:hexane = 1:1:6) diluted in hexane over the entire device and volatilizing the solvents.

Evaluation of single-element stretchable hybrid device

Strain distribution was analyzed through digital image correlation (DIC) analysis using random patterns. A random pattern was formed by spraying black-body spray on the single-element device shown in Figures 2A and S1. The patterned test devices were subjected to uniaxial strain at a rate of 1 mm/s. The process was captured using a video camera. The video was converted into a series of images at 1-s intervals and analyzed using DIC analysis software (Ncorr, MATLAB).

The LM paste wiring used for comparing the wiring characteristics was fabricated through stencil mask application. Monophasic LM is difficult to pattern with this application owing to its low viscosity. Hence, the wiring was fabricated by direct patterning using a dispenser. A 0-Ω resistor was mounted on both devices after drawing the wiring and fixed with an adhesive (Sili-poxy, Smooth-on). The wiring resistance was measured using an LCR meter (ZM2376, NF Corporation).

The sensor output values were obtained using an Arduino Uno as the master for I2C communication with the IMUs. Constant angular velocity and acceleration were provided by a rate table (RT-02-360-S12, COSMATE).

Data collection

Knot-shape recognition

The output values of the inertial sensors on the ribbon device were acquired via I2C communication using MPU6500, with Arduino Uno as the master, at a sampling rate of 200 Hz (Data S4). The start and end of data recording were determined by the experimenter. For each class, 110 datasets were obtained with a single participant.

Finger-writing recognition

The output values of the inertial sensors on the finger-writing device were acquired via I2C communication with MPU6500, with Arduino Uno as the master, at a sampling rate of 30 Hz. Finger-writing devices were used with an external multiplexer circuit. The start and end of data recording were determined using the acceleration threshold method (Figure S11), and the range from the "Beginning of gesture" to the "End of gesture" step and 40 steps before and after the range were processed as one character (Data S5). A total of 60 data samples were obtained for each class by 2 participants, resulting in a total of 120 datasets for each class.

Sign-language recognition

The output of the sign-language device was acquired at a sampling rate of 40 Hz via I2C communication using Arduino Uno as the master and controlled by a multiplexer mounted on the device. Two Arduino Uno units were used to simultaneously acquire data from the devices on the left and right hands. The start and end of data recording were determined through the same method used for finger-writing recognition (Data S6). Sixty datasets were acquired for each class for a single participant.

Data preprocessing

The acquired data comprised the acceleration matrix $\boldsymbol{a}$ and angular velocity matrix ω.

$$\boldsymbol{a} = \{\boldsymbol{a_{x1}}, \boldsymbol{a_{y1}}, \boldsymbol{a_{z1}}, \cdots \boldsymbol{a_{zk}}\},$$

$$\boldsymbol{a_m} = \{a_1, a_2 \cdots a_n\} \; (m = x1, y1, z1, \cdots zk),$$

$$\omega = \{\omega_{x1}, \omega_{y1}, \omega_{z1}, \cdots \omega_{zk}\},$$

$$\omega_m = \{\omega_1, \omega_2 \cdots \omega_n\} \; (m = x1, y1, z1, \cdots zk),$$

where k indicates the number of sensors on the system, and n indicates the number of steps in the time direction.

Knot-shape recognition

In knot recognition, $k = 2$. With the following equation, the acceleration $\boldsymbol{a}$ and angular velocity ω of each axis were normalized using the upper and lower measurement limits of the sensors (a_{max}, ω_{max} and a_{min}, ω_{min}, respectively).

$$\boldsymbol{a}_{norm} = \frac{\boldsymbol{a}}{(|a_{max}| + |a_{min}|)/2}$$

$$\omega_{norm} = \frac{\omega}{(|\omega_{max}| + |\omega_{min}|)/2}$$

The shape input to machine learning was set to (4,000,12), and data with $n < 4{,}000$ were padded with 0 to account for the missing data portion. The standardized data were then divided into 100 training data samples and 10 test data samples.

The following augmented datasets $\boldsymbol{a}_{aug}$ and ω_{aug} were generated by swapping the positions of the two sensors and reversing the signs of the x and y axes for the 100 training data samples:

$$\boldsymbol{a}_{aug} = \{-\boldsymbol{a}_{x2}, -\boldsymbol{a}_{y2}, \boldsymbol{a}_{z2}, -\boldsymbol{a}_{x1}, -\boldsymbol{a}_{y1}, \boldsymbol{a}_{z1}\}$$

$$\omega_{aug} = \{-\omega_{x2}, -\omega_{y2}, \omega_{z2}, -\omega_{x1}, -\omega_{y1}, \omega_{z1}\}$$

This corresponds to flipping the orientations of the left and right sides of the device before starting the tying motion. In addition, data were augmented by applying white noise to both the acquired data and inverted augmented data. Thus, 4,000 data samples (400 for each class) were used for the training.

Finger-writing recognition

Gravitational acceleration was removed from the acceleration data by using the following high-pass filter with $\alpha = 0.8$:

$$a_n = (1 - \alpha)a_{n-1} + \alpha a_n$$

The acceleration $\boldsymbol{a}$ and angular velocity $\boldsymbol{\omega}$ along each axis of the acquired data were standardized using the mean values a_{ave}, ω_{ave} and SDs $\sigma_{\boldsymbol{a}}, \sigma_{\omega}$ with the following equations:

$$\boldsymbol{a}_{std} = \frac{\boldsymbol{a} - a_{ave}}{\sigma_{\boldsymbol{a}}}$$

$$\omega_{std} = \frac{\boldsymbol{\omega} - \omega_{ave}}{\sigma_{\omega}}$$

The input shape for machine learning was set to (250,24) to match the shapes of data of different lengths. The data with $n < 250$ were padded with zeros. Finally, 100 data samples for each class were used for the training.

Sign-language recognition

The acquired data were divided into 40 training data samples and 20 test data samples. Unlike finger-writing recognition, data were used for sign-language recognition without removal of gravity acceleration.

The acceleration $\boldsymbol{a}$ and angular velocity $\boldsymbol{\omega}$ along each axis of the acquired data were standardized using the mean values a_{ave}, ω_{ave} and SDs $\sigma_{\boldsymbol{a}}, \sigma_{\omega}$ with the following equations:

$$\boldsymbol{a}_{std} = \frac{\boldsymbol{a} - a_{ave}}{\sigma_{\boldsymbol{a}}}$$

$$\omega_{std} = \frac{\boldsymbol{\omega} - \omega_{ave}}{\sigma_{\omega}}$$

The input shape for machine learning was set to (250,84) to match the shapes of data with different lengths. The data with $n < 250$ were padded with zero. The augmented data were generated from the training data by applying white noise and deforming the data in the time direction after preprocessing. Thus, 80 data samples were used for training for each class.

Optimization and training of the model

The models for the three classification tasks were examined using stratified 3-fold cross-validation. The training data were divided into three parts, two of which were used for training and one for validation. All combinations of the three parts of the data were trained, and the average accuracy and macro-F1 score were calculated. The data were divided to make the proportion of each class in the three partitions equal. Training was performed using the hyperparameters of the optimized model with 10 data samples from the training data as validation data.

Visualization of classification performance through clustering

Clustering was performed by dimensionality compression using principal-component analysis (PCA). t-Distributed stochastic neighbor embedding (t-SNE), which is used for the planar projection of multidimensional data, and it was used as the visualization method.[42] All data were flattened to a 1D vector and then dimensionally compressed up to 100 dimensions using PCA. The principal components were selected for visualization in the order of their contribution from the compressed principal components. Finally, principal components in the range with a total contribution of $\geq 80\%$ were used for visualization by t-SNE.

Controlling the smart assistant with sign-language recognition system

A schematic of controlling the smart assistant using the sign-language recognition system is shown in Figure S22. Google Assistant SDK for Python (Github: https://github.com/googlesamples/assistant-sdk-python) was used as the smart assistant. Google Assistant was installed on a virtual Linux machine built on a Windows PC using Windows Subsystem for Linux 2 (WSL2) and customized to support the text input. The motion data of the sign language were converted into text data in real time by a machine learning-based sign-language recognition system running on Windows, and sent to Google Assistant on WSL2 using transmission control protocol/Internet protocol communication. The ceiling lights were operated by SwitchBot (SwitchBot Company) and SwitchBot hub mini (SwitchBot Company), which are associated with Google Assistant.

Experiments with human research participants

The research protocol was approved by the ethics committee of the Yokohama National University Graduate School of Engineering Science (no. 2020-16, approved on February 12, 2021).

SUPPLEMENTAL INFORMATION

Supplemental information can be found online at https://doi.org/10.1016/j.device.2024.100496.

ACKNOWLEDGMENTS

This research was supported by the Japan Science and Technology Agency (JST) Advanced Integrated Intelligence Platform Project (no. JPMJCR22U2) and the Japan Society for the Promotion of Science (JSPS) KAKENHI Grant-in-Aid for Transformative Research Areas (no. 24H00890).

AUTHOR CONTRIBUTIONS

Conceptualization, Y. Isano, R.M., T.H., and H.O. Methodology, Y. Isano, M.T., Y.K., and Y.M. Software, Y. Isano, M.T., Y.K., and T.T. Investigation, Y. Isano, M.T., and Y. Isoda. Data curation, Y. Isano, M.T., and Y. Isoda. Writing – original draft, Y. Isano. Writing – review & editing, Y.M., K.K., and H.O. Funding acquisition, K.K. and H.O. Supervision, K.K. and H.O.

DECLARATION OF INTERESTS

The authors declare no competing interests.

Received: March 15, 2024
Revised: June 3, 2024
Accepted: July 8, 2024
Published: August 7, 2024

REFERENCES

1. Rogers, J.A., Someya, T., and Huang, Y. (2010). Materials and mechanics for stretchable electronics. Science *327*, 1603–1607. https://doi.org/10.1126/SCIENCE.1182383.
2. Lee, Y., Chung, J.W., Lee, G.H., Kang, H., Kim, J.Y., Bae, C., Yoo, H., Jeong, S., Cho, H., Kang, S.G., et al. (2021). Standalone real-time health monitoring patch based on a stretchable organic optoelectronic system. Sci. Adv. *7*, eabg9180. https://doi.org/10.1126/SCIADV.ABG9180.
3. Xu, S., Zhang, Y., Jia, L., Mathewson, K.E., Jang, K.I., Kim, J., Fu, H., Huang, X., Chava, P., Wang, R., et al. (2014). Soft microfluidic assemblies of sensors, circuits, and radios for the skin. Science *344*, 70–74. https://doi.org/10.1126/SCIENCE.1250169.

4. Liu, Y., Norton, J.J.S., Qazi, R., Zou, Z., Ammann, K.R., Liu, H., Yan, L., Tran, P.L., Jang, K.I., Lee, J.W., et al. (2016). Epidermal mechano-acoustic sensing electronics for cardiovascular diagnostics and human-machine interfaces. Sci. Adv. *2*, e1601185. https://doi.org/10.1126/SCIADV.1601185.
5. Sani, E.S., Xu, C., Wang, C., Song, Y., Min, J., Tu, J., Solomon, S.A., Li, J., Banks, J.L., Armstrong, D.G., and Gao, W. (2023). A stretchable wireless wearable bioelectronic system for multiplexed monitoring and combination treatment of infected chronic wounds. Sci. Adv. *9*, eadf7388. https://doi.org/10.1126/SCIADV.ADF7388.
6. Zheng, C., Li, W., Shi, Y., Wei, S., Liu, K., Cheng, J., Ji, L., and Lu, Y. (2023). Stretchable self-adhesive and self-powered smart bandage for motion perception and motion intention recognition. Nano Energy *109*, 108245. https://doi.org/10.1016/J.NANOEN.2023.108245.
7. Lee, H., Lee, S., Kim, J., Jung, H., Yoon, K.J., Gandla, S., Park, H., and Kim, S. (2023). Stretchable array electromyography sensor with graph neural network for static and dynamic gestures recognition system. npj Flex. Electron. *7*, 20. https://doi.org/10.1038/s41528-023-00246-3.
8. Liu, Y., Jiang, X., Yu, X., Ye, H., Ma, C., Wang, W., and Hu, Y. (2023). A wearable system for sign language recognition enabled by a convolutional neural network. Nano Energy *116*, 108767. https://doi.org/10.1016/J.NANOEN.2023.108767.
9. Li, K., Zhang, D., Zhang, H., Wang, D., Xu, Z., Cai, H., and Xia, H. (2023). Triboelectric nanogenerators based on super-stretchable conductive hydrogels with the assistance of deep-learning for handwriting recognition. ACS Appl. Mater. Interfaces *15*, 32993–33002. https://doi.org/10.1021/ACSAMI.3C06597.
10. Kim, K.K., Kim, M., Pyun, K., Kim, J., Min, J., Koh, S., Root, S.E., Kim, J., Nguyen, B.N.T., Nishio, Y., et al. (2022). A substrate-less nanomesh receptor with meta-learning for rapid hand task recognition. Nat. Electron. *6*, 64–75. https://doi.org/10.1038/s41928-022-00888-7.
11. Zhou, Z., Chen, K., Li, X., Zhang, S., Wu, Y., Zhou, Y., Meng, K., Sun, C., He, Q., Fan, W., et al. (2020). Sign-to-speech translation using machine-learning-assisted stretchable sensor arrays. Nat. Electron. *3*, 571–578. https://doi.org/10.1038/s41928-020-0428-6.
12. Karipoth, P., Christou, A., Pullanchiyodan, A., and Dahiya, R. (2022). Bioinspired inchworm- and earthworm-like soft robots with intrinsic strain sensing. Adv. Intell. Syst. *4*, 2100092. https://doi.org/10.1002/AISY.202100092.
13. Hu, X., Yang, F., Wu, M., Sui, Y., Guo, D., Li, M., Kang, Z., Sun, J., and Liu, J. (2022). A super-stretchable and highly sensitive carbon nanotube capacitive strain sensor for wearable applications and soft robotics. Adv. Mater. Technol. *7*, 2100769. https://doi.org/10.1002/ADMT.202100769.
14. Zhang, S., Suresh, L., Yang, J., Zhang, X., and Tan, S.C. (2022). Augmenting sensor performance with machine learning towards smart wearable sensing electronic systems. Adv. Intell. Syst. *4*, 2100194. https://doi.org/10.1002/AISY.202100194.
15. Wang, M., Wang, T., Luo, Y., He, K., Pan, L., Li, Z., Cui, Z., Liu, Z., Tu, J., Chen, X., et al. (2021). Fusing stretchable sensing technology with machine learning for human–machine interfaces. Adv. Funct. Mater. *31*, 2008807. https://doi.org/10.1002/ADFM.202008807.
16. Wang, Y., Tang, T., Xu, Y., Bai, Y., Yin, L., Li, G., Zhang, H., Liu, H., and Huang, Y.A. (2021). All-weather, natural silent speech recognition via machine-learning-assisted tattoo-like electronics. npj Flex. Electron. *5*, 20. https://doi.org/10.1038/s41528-021-00119-7.
17. Yan, Z., Pan, T., Wang, D., Li, J., Jin, L., Huang, L., Jiang, J., Qi, Z., Zhang, H., Gao, M., et al. (2019). Stretchable micromotion sensor with enhanced sensitivity using serpentine layout. ACS Appl. Mater. Interfaces *11*, 12261–12271. https://doi.org/10.1021/ACSAMI.8B22613.
18. Trung, T.Q., and Lee, N.-E. (2017). Recent progress on stretchable electronic devices with intrinsically stretchable components. Adv. Mater. *29*, 1603167. https://doi.org/10.1002/ADMA.201603167.
19. Byun, J., Oh, E., Lee, B., Kim, S., Lee, S., and Hong, Y. (2017). A single droplet-printed double-side universal soft electronic platform for highly integrated stretchable hybrid electronics. Adv. Funct. Mater. *27*, 1701912. https://doi.org/10.1002/ADFM.201701912.
20. Ozutemiz, K.B., Wissman, J., Ozdoganlar, O.B., and Majidi, C. (2018). EGaIn–metal interfacing for liquid metal circuitry and microelectronics integration. Adv. Mater. Interfaces *5*, 1701596. https://doi.org/10.1002/ADMI.201701596.
21. Li, G., and Lee, D.W. (2017). An advanced selective liquid-metal plating technique for stretchable biosensor applications. Lab Chip *17*, 3415–3421. https://doi.org/10.1039/c7lc00768j.
22. Chang Yang, J., Lee, S., Soo Ma, B., Kim, J., Song, M., Yeong Kim, S., Won Kim, D., Kim, T.-S., and Park, S. (2022). Geometrically engineered rigid island array for stretchable electronics capable of withstanding various deformation modes. Sci. Adv. *8*, eabn3863. https://doi.org/10.1126/sciadv.abn3863.
23. Kim, D.H., Lu, N., Ma, R., Kim, Y.S., Kim, R.H., Wang, S., Wu, J., Won, S.M., Tao, H., Islam, A., et al. (2011). Epidermal electronics. Science *333*, 838–843. https://doi.org/10.1126/SCIENCE.1206157.
24. Lin, R., Li, Y., Mao, X., Zhou, W., and Liu, R. (2019). Hybrid 3D printing all-in-one heterogenous rigidity assemblies for soft electronics. Adv. Mater. Technol. *4*, 1900614. https://doi.org/10.1002/ADMT.201900614.
25. Jang, K.I., Li, K., Chung, H.U., Xu, S., Jung, H.N., Yang, Y., Kwak, J.W., Jung, H.H., Song, J., Yang, C., et al. (2017). Self-assembled three dimensional network designs for soft electronics. Nat. Commun. *8*, 15894. https://doi.org/10.1038/ncomms15894.
26. Mahmood, M., Mzurikwao, D., Kim, Y.-S., Lee, Y., Mishra, S., Herbert, R., Duarte, A., Ang, C.S., and Yeo, W.-H. (2019). Fully portable and wireless universal brain–machine interfaces enabled by flexible scalp electronics and deep learning algorithm. Nat. Mach. Intell. *1*, 412–422. https://doi.org/10.1038/s42256-019-0091-7.
27. Jiang, Y., Ji, S., Sun, J., Huang, J., Li, Y., Zou, G., Salim, T., Wang, C., Li, W., Jin, H., et al. (2023). A universal interface for plug-and-play assembly of stretchable devices. Nature *614*, 456–462. https://doi.org/10.1038/s41586-022-05579-z.
28. Naserifar, N., Leduc, P.R., and Fedder, G.K. (2016). Material gradients in stretchable substrates toward integrated electronic functionality. Adv. Mater. *28*, 3584–3591. https://doi.org/10.1002/ADMA.201505818.
29. Kim, M.S., Kim, S., Choi, J., Kim, S., Han, C., Lee, Y., Jung, Y., Park, J., Oh, S., Bae, B.S., et al. (2022). Stretchable printed circuit board based on leak-free liquid metal interconnection and local strain control. ACS Appl. Mater. Interfaces *14*, 1826–1837. https://doi.org/10.1021/ACSAMI.1C16177.
30. Daalkhaijav, U., Yirmibesoglu, O.D., Walker, S., and Mengüç, Y. (2018). Rheological modification of liquid metal for additive manufacturing of stretchable electronics. Adv. Mater. Technol. *3*, 1700351. https://doi.org/10.1002/ADMT.201700351.
31. Cao, Y., Zhang, G., Zhang, Y., Yue, M., Chen, Y., Cai, S., Xie, T., and Feng, X. (2018). Direct fabrication of stretchable electronics on a polymer substrate with process-integrated programmable rigidity. Adv. Funct. Mater. *28*, 1804604. https://doi.org/10.1002/ADFM.201804604.
32. Hermanis, A., Cacurs, R., and Greitans, M. (2016). Acceleration and magnetic sensor network for shape sensing. IEEE Sens. J. *16*, 1271–1280. https://doi.org/10.1109/JSEN.2015.2496283.
33. Liu, L., Zhao, C., Guo, M., Chen, Y., Wu, Y., Li, Z., Li, Y., Xiang, D., Li, H., and Wang, L. (2023). Spider-web inspired self-healing, adhesive, injectable conductive hydrogel for human motion monitoring and shape recognition. Colloids Surf. A Physicochem. Eng. Asp. *672*, 131739. https://doi.org/10.1016/J.COLSURFA.2023.131739.
34. Shahabi, E., Visentin, F., Mondini, A., and Mazzolai, B. (2023). Octopus-inspired suction cups with embedded strain sensors for object recognition. Adv. Intell. Syst. *5*, 2200201. https://doi.org/10.1002/AISY.202200201.
35. Shi, Q., Sun, Z., Le, X., Xie, J., and Lee, C. (2023). Soft robotic perception system with ultrasonic auto-positioning and multimodal sensory

intelligence. ACS Nano *17*, 4985–4998. https://doi.org/10.1021/ACS-NANO.2C12592.

36. Bhirangi, R., Hellebrekers, T., Majidi, C., and Gupta, A. (2021). ReSkin: Versatile, Replaceable, Lasting Tactile Skins. Preprint at arXiv. https://doi.org/10.48550/arXiv.2111.00071.
37. Cho, H., Lee, I., Jang, J., Kim, J.H., Lee, H., Park, S., and Wang, G. (2023). Real-time finger motion recognition using skin-conformable electronics. Nat. Electron. *6*, 619–629. https://doi.org/10.1038/s41928-023-01012-z.
38. Hughes, J., Spielberg, A., Chounlakone, M., Chang, G., Matusik, W., and Rus, D. (2020). A simple, inexpensive, wearable glove with hybrid resistive-pressure sensors for computational sensing, proprioception, and task identification. Adv. Intell. Syst. *2*, 2000002. https://doi.org/10.1002/AISY.202000002.
39. Jin, L., Li, Z., Liu, Z., Richardson, B., Zheng, Y., Xu, L., Chen, Z., Zhai, H., Kim, H., Song, Q., et al. (2022). Flexible unimodal strain sensors for human motion detection and differentiation. npj Flex. Electron. *6*, 74. https://doi.org/10.1038/s41528-022-00205-4.
40. Liu, Z.T., Wong, D.P.Y., and Chou, P.H. (2020). An imu-based wearable ring for on-surface handwriting recognition. In 2020 International Symposium on VLSI Design, Automation and Test, VLSI-DAT 2020 (Institute of Electrical and Electronics Engineers Inc.). https://doi.org/10.1109/VLSI-DAT49148.2020.9196479.
41. Zhang, H., Chen, L., Zhang, Y., Hu, R., He, C., Tan, Y., and Zhang, J. (2022). A wearable real-time character recognition system based on edge computing-enabled deep learning for air-writing. J. Sens. *2022*, 507706. https://doi.org/10.1155/2022/8507706.
42. Wen, F., Zhang, Z., He, T., and Lee, C. (2021). AI enabled sign language recognition and VR space bidirectional communication using triboelectric smart glove. Nat. Commun. *12*, 5378. https://doi.org/10.1038/s41467-021-25637-w.
43. Wang, M., Yan, Z., Wang, T., Cai, P., Gao, S., Zeng, Y., Wan, C., Wang, H., Pan, L., Yu, J., et al. (2020). Gesture recognition using a bioinspired learning architecture that integrates visual data with somatosensory data from stretchable sensors. Nat. Electron. *3*, 563–570. https://doi.org/10.1038/s41928-020-0422-z.
44. Moin, A., Zhou, A., Rahimi, A., Menon, A., Benatti, S., Alexandrov, G., Tamakloe, S., Ting, J., Yamamoto, N., Khan, Y., et al. (2020). A wearable biosensing system with in-sensor adaptive machine learning for hand gesture recognition. Nat. Electron. *4*, 54–63. https://doi.org/10.1038/s41928-020-00510-8.
45. Ahmed, M.A., Zaidan, B.B., Zaidan, A.A., Alamoodi, A.H., Albahri, O.S., Al-Qaysi, Z.T., Albahri, A.S., and Salih, M.M. (2021). Real-time sign language framework based on wearable device: analysis of MSL, DataGlove, and gesture recognition. Soft Comput. *25*, 11101–11122. https://doi.org/10.1007/S00500-021-05855-6.
46. Fang, B., Sun, F., Liu, H., and Liu, C. (2018). 3D human gesture capturing and recognition by the IMMU-based data glove. Neurocomputing *277*, 198–207. https://doi.org/10.1016/J.NEUCOM.2017.02.101.